atmosphere

MDPI

Supplementary Materials: Performance of Simulated Effective Radius and Cloud Top Height Fields in Selected Case Studies

Meelis J. Zidikheri * and Chris Lucas

Bureau of Meteorology, Melbourne 3001, Australia; chris.lucas@bom.gov.au
* Correspondence: meelis.zidikheri@bom.gov.au

1. Introduction

In this supplementary section, we evaluate the performance of the volcanic ash ensemble filtering system [1] with respect to the effective radius and cloud top height fields in two case studies, namely the 13 February 2014 Kelut eruption and the 4 November 2015 Rinjani eruption (the performance of the mass load field is evaluated in Section 4 of the main manuscript). The evaluation is based on comparing the spatial patterns of these ash cloud properties obtained with the ensemble filtering system to those retrieved by the VOLCAT system [2] from satellite data; the results are also compared to reference runs in which there is no ensemble filtering. Different formulations of the source term are considered for the ensemble filtered runs, namely a cylindrical source centered at the volcano and initialized at the eruption start time (SRC), a distal source based on directly inserting satellite data (DIST(VARH)), and a hybrid scheme in which some ensemble members are of SRC type and others of DIST(VARH) type (SRC-DIST). In addition, for each source type, we consider two types of observations for the purposes of initialization and optimization, namely detections (which are simply binary fields indicating presence or absence of retrievals) and detailed retrievals of ash cloud properties. These different formulations are described in detail in Section 2 of the main manuscript.

2. Evaluation of Effective Radius

The simulated effective radius field, $\rho(\boldsymbol{x})$, is computed from the relationship [3] [2]

$$\rho(\boldsymbol{x}) = \mu_r(\boldsymbol{x}) exp\left[\frac{5}{2}(log\ \sigma_r)^2\right], \tag{S1}$$

where $\mu_r(\boldsymbol{x})$ is the mean geometric radius field, σ_r = 2.1 μm is the geometric standard deviation, and $\boldsymbol{x}$ is a position vector (latitude, longitude). The mean particle radius field $\mu_r(\boldsymbol{x})$ in Equation (S1) is determined by optimal fitting to the relationship [4]

$$g(r,\boldsymbol{x}) = \frac{r^2 \exp[-\frac{(\ln r - \ln \mu_r(\boldsymbol{x}))^2}{2(\ln \sigma_r)^2}]}{\int_0^R \left\{r^2 \exp[-\frac{(\ln r - \ln \mu_r(\boldsymbol{x}))^2}{2(\ln \sigma_r)^2}]\right\} dr}, \tag{S2}$$

where $g(r,\boldsymbol{x})$ is the normalised particle size mass distribution, which is determined from the dispersion model by computing the proportion of mass comprising particles with radius r at each grid point location $\boldsymbol{x}$ with some volcanic ash. The particles sizes are grouped into ten bins in the range [0, R], where R = 50 μm.

2.1. 13 February 2014 Kelut Case Study

Figure S1 shows the spatial patterns of effective radius at 14/0130 UTC, which occurs during the analysis phase in which the ensemble is filtered relative to the observations. The VOLCAT retrieval at this timestep indicates large effective radii, close to the retrieval limit of 15 μm [2], over most of the ash cloud except for a region just to the south of the volcano in which smaller effective radii are retrieved. The reference run, which utilizes a default particle size distribution based on the study of Hobbs [5], also produces a cloud with large effective radii although the overall ash cloud location differs somewhat from

that obtained by the VOLCAT retrieval. The cylindrical source runs (SRC) produce patterns with large effective radii in the middle of the ash cloud and smaller effective radii elsewhere. None of these patterns agree very well with retrievals, although it could be argued that the agreement if better if one considers that the areas with very large effective radii, which are mostly to the north of 9°S in Figure S1c,d will not be expected to show up in the VOLCAT retrievals due to the effective radius possibly exceeding the retrieval limit. The distal source runs (DIST(VARH)), as expected, display better agreement with satellite observations with respect to ash locations. The detection-based run (e) predicts large effective radii, although the distribution is completely uniform as a consequence of the formulation used when retrievals are not employed (see Section 2.3.2 of the main manuscript). The retrieval-based run (f), in addition to better representing the locations with ash, also displays an effective radius distribution that is in closer agreement with the VOLCAT retrieval. The hybrid runs (SRC-DIST) also represent the ash locations quite well. The retrieval-based run (h) is broadly like the DIST(VARH) type run and agrees reasonably well the VOLCAT retrieval. The detection-based run, however, does not reproduce the VOLCAT pattern very well.

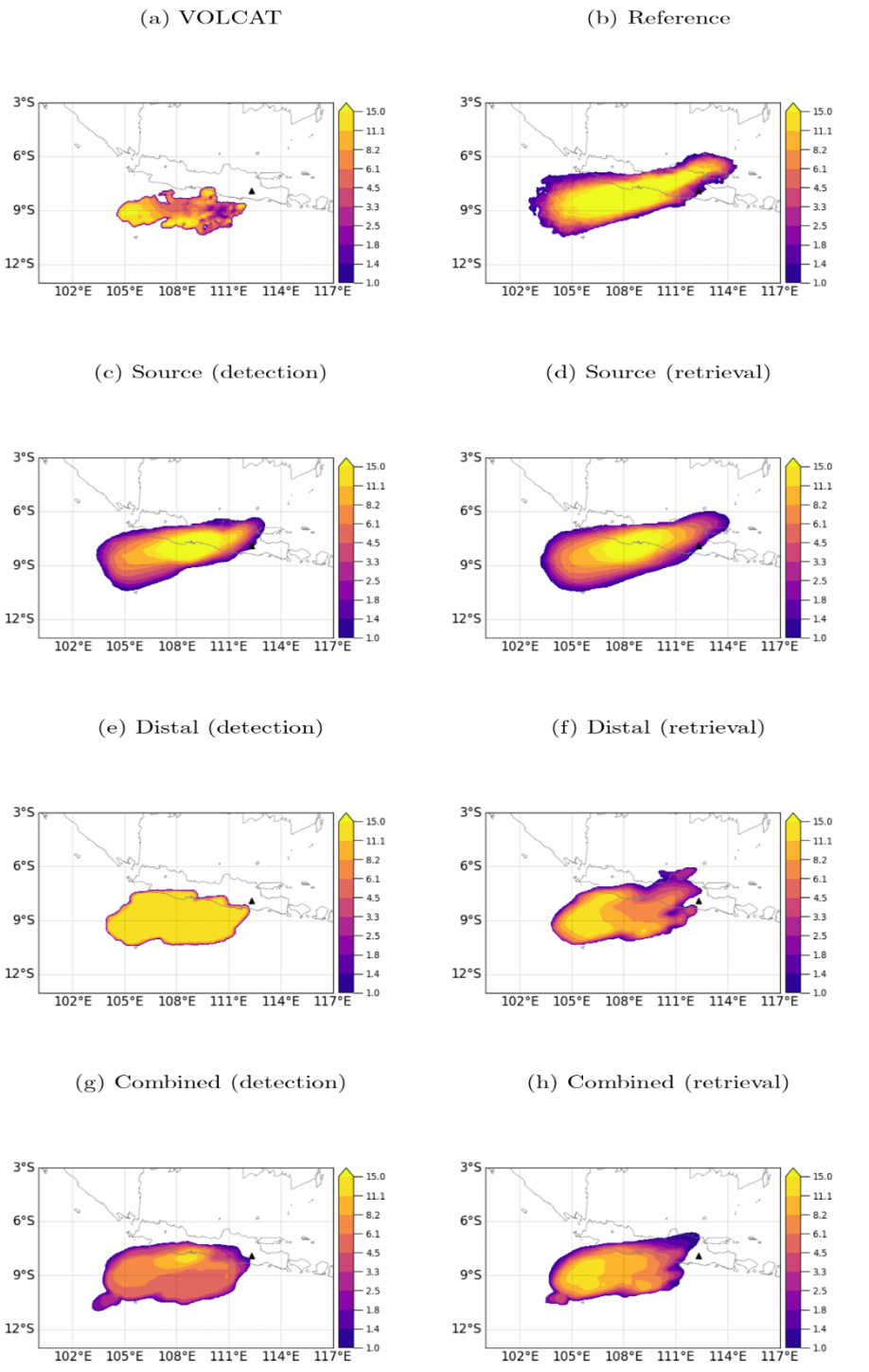

Figure S1. Ensemble mean effective radius fields in the 13 February 2014 Kelut eruption case study at 14/0130 UTC for (**a**) VOLCAT retrieval, (**b**) reference run, (**c**) cylindrical source run with detection-based optimization, (**d**) cylindrical source run with retrieval-based optimization, (**e**) distal source run with detection-based initialization and optimization, (**f**) distal source run with retrieval-based initialization and optimization, (**g**) hybrid source run using detections, and (**h**) hybrid source run using retrievals.

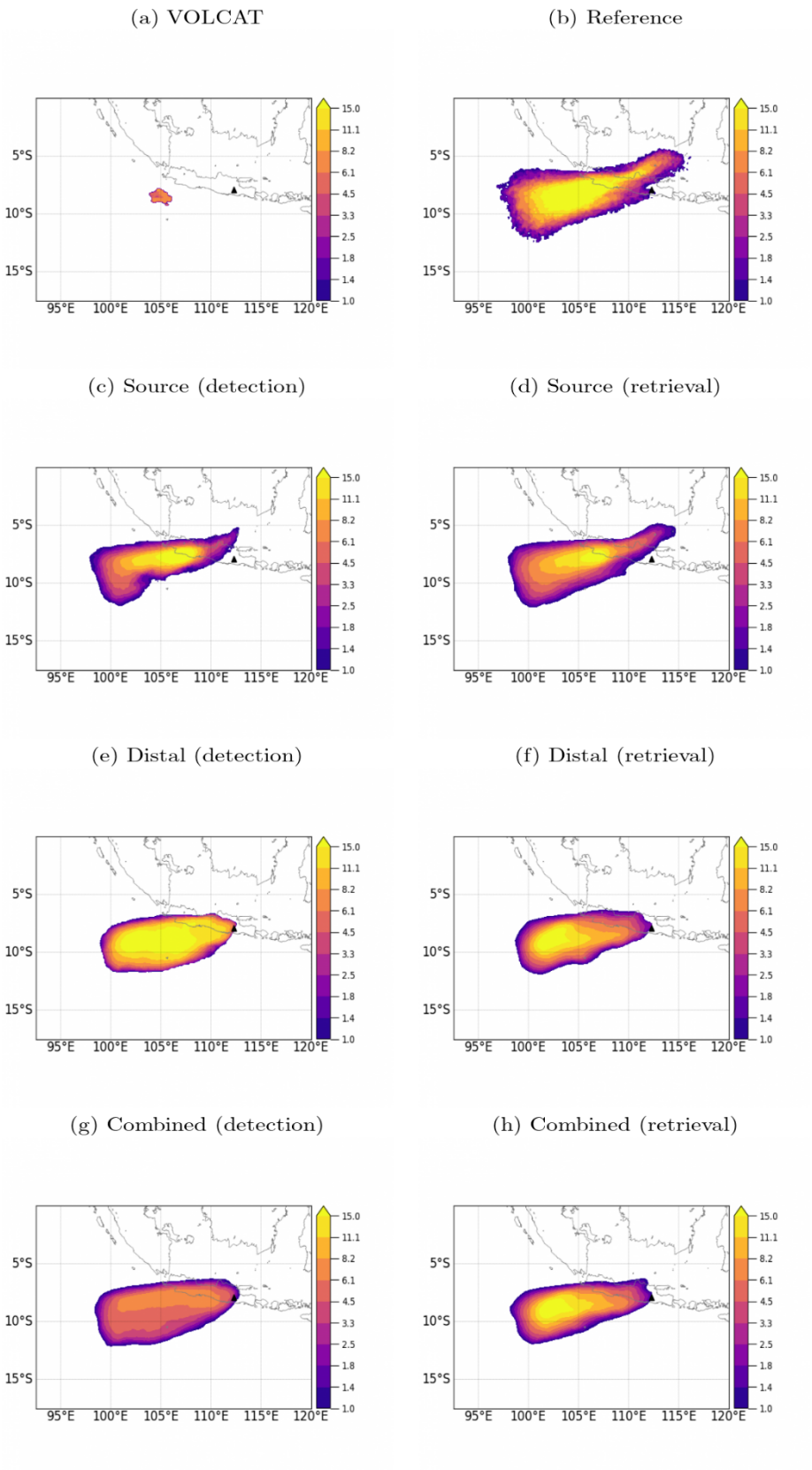

Figure S2. Same as in Figure S2 but for the 14/0830 timestep.

Figure S2 shows the effective radius patterns at 14/0830 UTC, which occurs during the forecast phase of the algorithm, in which observations are no longer being utilized by the system. As discussed in the main manuscript, the extent of the ash cloud is not well

captured by the VOLCAT retrievals by this time; only a small region centred at 105°E 9°S is identified to contain ash, but the ash cloud was probably much more extensive. The very large effective radii identified in the retrievals at an earlier time (Figure S1) is one possible reason that the ash cloud was not well detected by the system. The reference run indicates large effective radii at this timestamp as well, which supports this hypothesis although that does not account for the small region of detected ash in the VOLCAT retrieval. The SRC-type runs display regions of large effective radii in the middle of the ash cloud, and lower effective radii elsewhere, consistent with results from an earlier timestep (Figure S1). The large-effective-radius region overlaps the region retrieved by VOLCAT, but the modelled effective radius is significantly larger. The DIST(VARH) type runs are also consistent with the results from Figure S1. The detection-based run has a more uniform distribution of effective radii, while the retrieval-based run has larger radii upstream (nearer to the source). Both results are not completely consistent with the VOLCAT retrieval although the retrieval-based run could possibly be the better representation if we assume that the region with large effective radii would not be retrievable by VOLCAT. For the hybrid formulation (SRC-DIST), the retrieval-based run has a very similar performance to the DIST(VARH) run. The distribution of effective radii is somewhat different in the detection-based run. However, the region overlapping the region with VOLCAT retrievals does have similar effective radius values to the VOLCAT retrievals. Nonetheless, it is not completely clear whether this is just coincidence or a manifestation of improved model skill. The quantitative skill score results in Figure S2d of the main manuscript suggest that the hybrid scheme is not significantly superior to the other schemes in this case study, so the similar effective radius values in the overlapping region are quite likely a coincidence.

2.2 .4 November 2015 Rinjani Eruption

Figure S3 shows the results obtained for 4 November 2015 Rinjani eruption at 5/0730 UTC (i.e., on 5 November), which occurs during the analysis phase. The VOLCAT retrievals indicate moderate effective radii of around 3–5 μm over most of the cloud. The reference run, on the other hand, displays significantly larger effective radii (> 8 μm) over most of the ash cloud. In addition, the ash cloud coverage is not very well represented, with incorrect transport direction and too little ash downstream, as discussed in the main manuscript. The cylindrical source (SRC) runs improve the effective radius representation somewhat with more smaller particle sizes represented on average although the pattern of variation does not appear to be reproduced very well. The detection-based distal source (DIST(VARH)) run has too high a proportion of larger sized particles in the middle of the cloud although the cloud extent is reasonably well represented. The retrieval based DIST run, however, reproduces both cloud extent and the particle size range in the cloud quite well when compared to the VOLCAT retrieval. This is also true for the hybrid scheme (DIST-SRC) when employing retrievals. The hybrid scheme without retrievals seems to underestimate the particle sizes relative to the VOLCAT retrievals on average, however.

Figure S4 shows a timestep (5/1430 UTC) from the forecast phase of the Rinjani eruption. The ash cloud has dispersed more by this time and has been transported further to the south-west when compared to Figure S3. The effective radius is broadly in the 2–5 μm range in the ash cloud, although there are smaller regions with larger retrieved particle sizes. In the reference run, the ash cloud is mostly confined to the near-source region and the effective radii are quite large, as in the analysis step in Figure S3. The large sizes of particles might explain why there is very little ash mass in the downstream region in this simulation because larger particles will tend to fall quickly and be deposited before they can travel great distances. Particle size representation appears to improve in the SRC runs relative to the VOLCAT retrieval, with a high proportion of smaller particles in the simulated cloud. This is also true for the distal source runs (DIST(VARH)) although the average particle size appears to be somewhat lower than in the retrievals. The hybrid runs (SRC-DIST) represent effective radii very similarly to the purely distal (DIST) runs.

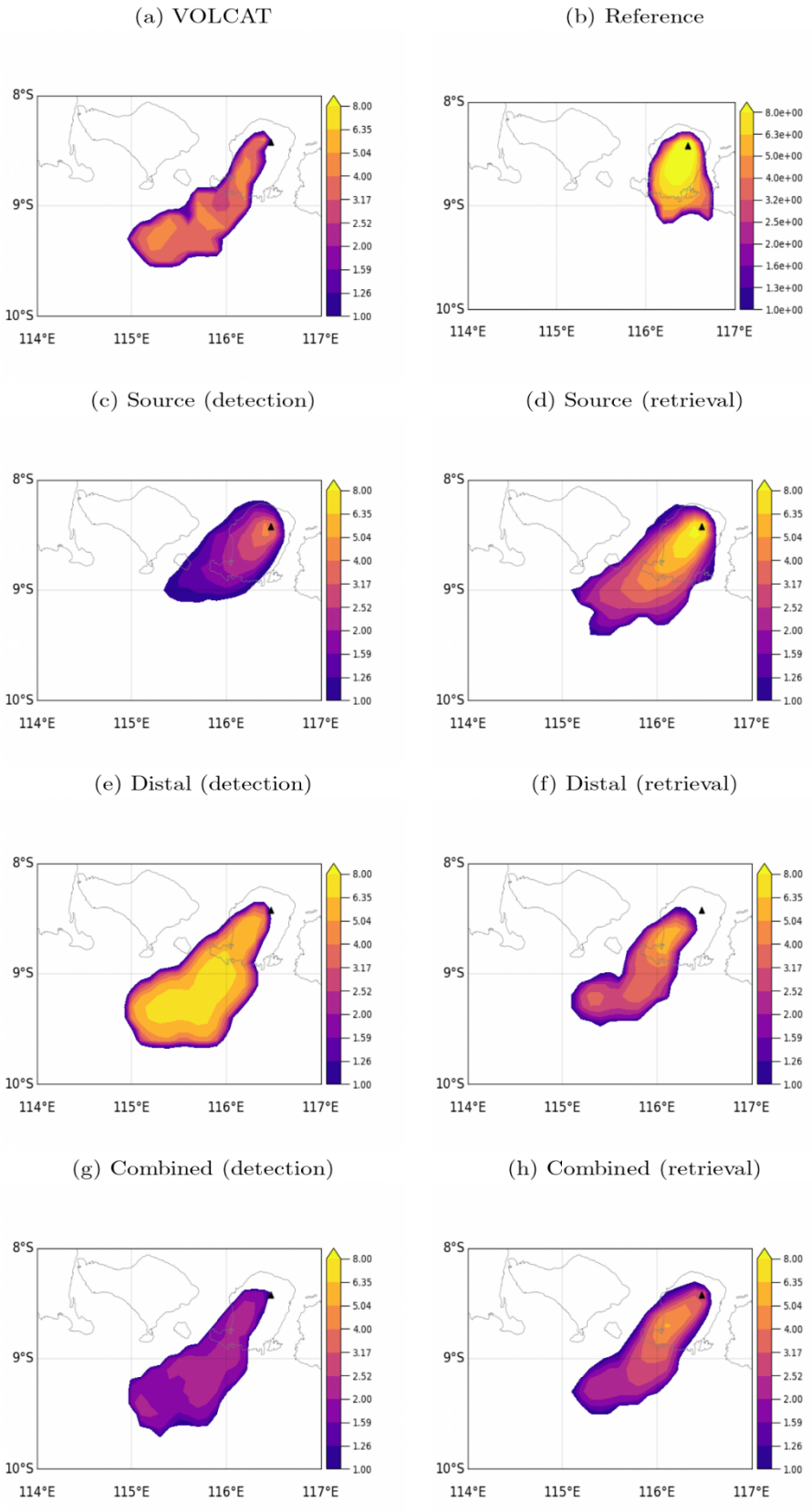

Figure S3. Same as in Figure S1 but for the 4 November Rinjani eruption at 5/0730 UTC.

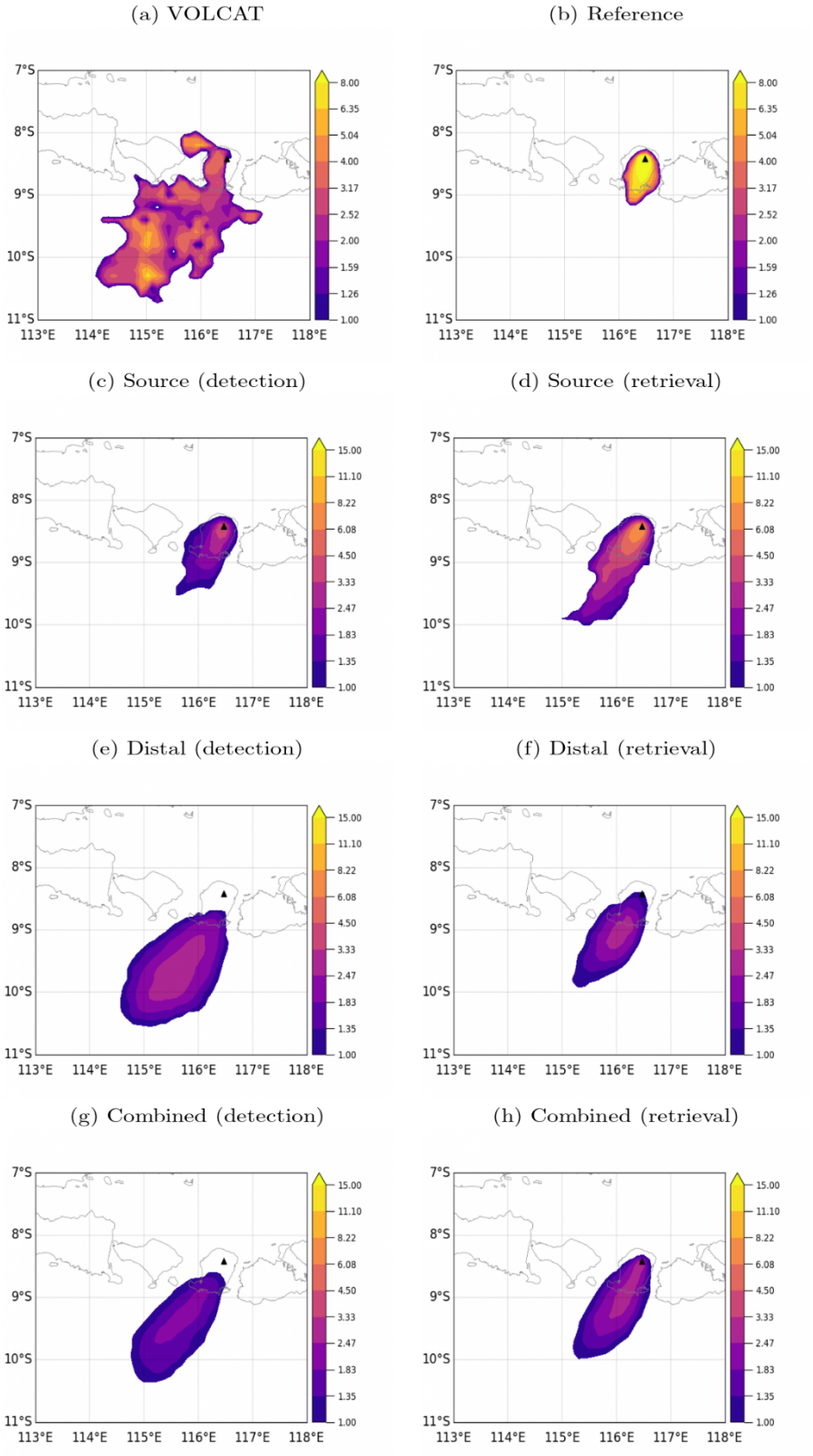

Figure S4. Same as in Figure S3 but for the 5/1430 UTC timestep.

3. Evaluation of Cloud Top Height

The cloud top height, $h_T(\boldsymbol{x})$, is determined from the dispersion model three-dimensional ash mass concentration field q($\boldsymbol{x}$, z) by finding the maximum value of z for which

$q(\boldsymbol{x}, z) > \varepsilon$, where ε is a threshold concentration value chosen to be equal to 1% of the peak concentration value at every grid point $\boldsymbol{x}$. The threshold value is somewhat arbitrary. If it is too small, however, spurious small concentration values associated with sampling error will tend to contaminate the results and if it is too large then the top height will be underestimated. We found that setting ε to be 1% of the peak concentration value at every grid point appeared to give reasonable results across many different case studies.

3.1. 13 February 2014 Kelut Case Study

Figure S5 shows the cloud top height results at 14/0130 UTC, which is part of the analysis phase in the Kelut case study. The VOLCAT retrieval indicates heights of 14–20 km near the leading edge of the cloud (downstream region) and lower heights elsewhere. These results are broadly consistent with other data associated with the Kelut eruption, which showed the top of the umbrella cloud to be just under 20 km [6]. However, emissions also appeared to reach as high as 26 km during the eruption [6], but these are not picked up by the VOLCAT retrieval. The reference and SRC runs show broadly similar patterns to each other, with altitudes exceeding 20 km in most of the south-western moving component of the ash cloud and lower altitudes in the north-eastern component of the ash cloud. Apart from differing from the VOLCAT retrieval in having a north-east component to the ash cloud, they also differ in the extent to which the high-altitude cloud is spread in the south-west component, with the VOLCAT retrievals only indicating very high altitudes near the leading edge of the cloud. The detection based DIST(VARH) run improves the overall representation of the ash cloud extent, but the cloud top height is uniformly over 20 km within the cloud. This is a consequence of the distal source formulation when there are no retrievals to identify cloud top height variations (see Section 2.3.2 of the main manuscript). The retrieval-based version, however, represents the cloud top height variations, in addition to the overall ash cloud location, quite well; this is because the retrievals are directly inserted into the system. The hybrid scheme (SRC-DIST) with retrievals also performs similarly while the detection-based version displays high altitudes through most of the cloud as in the SRC and DIST versions.

Figure S6 shows results from the Kelut case study at 14/0830 UTC, which occurs during the forecast phase. As noted previously, VOLCAT only detects a small region of the ash cloud at this time step (which is quite possibly related to the high values of the retrieved effective radii as noted in Section 1.1) with ash cloud top heights in the range 10–14 km. Ignoring the fact that the ash cloud extent is significantly larger than that in the VOLCAT retrievals, the reference run predicts the retrieved altitude quite well. The detection-based SRC run also predicts this altitude quite well, but the retrieval-based run underestimates the retrieved altitude for some reason (it is not clear why it is specifically the region with retrievals that is underestimated and not surrounding regions). Both the purely distal (DIST(VARH)) and hybrid schemes (SRC-DIST) overestimate the retrieved height. This is reflected in the poor Brier skill scores obtained in Figures S2 and S3 of the main manuscript.

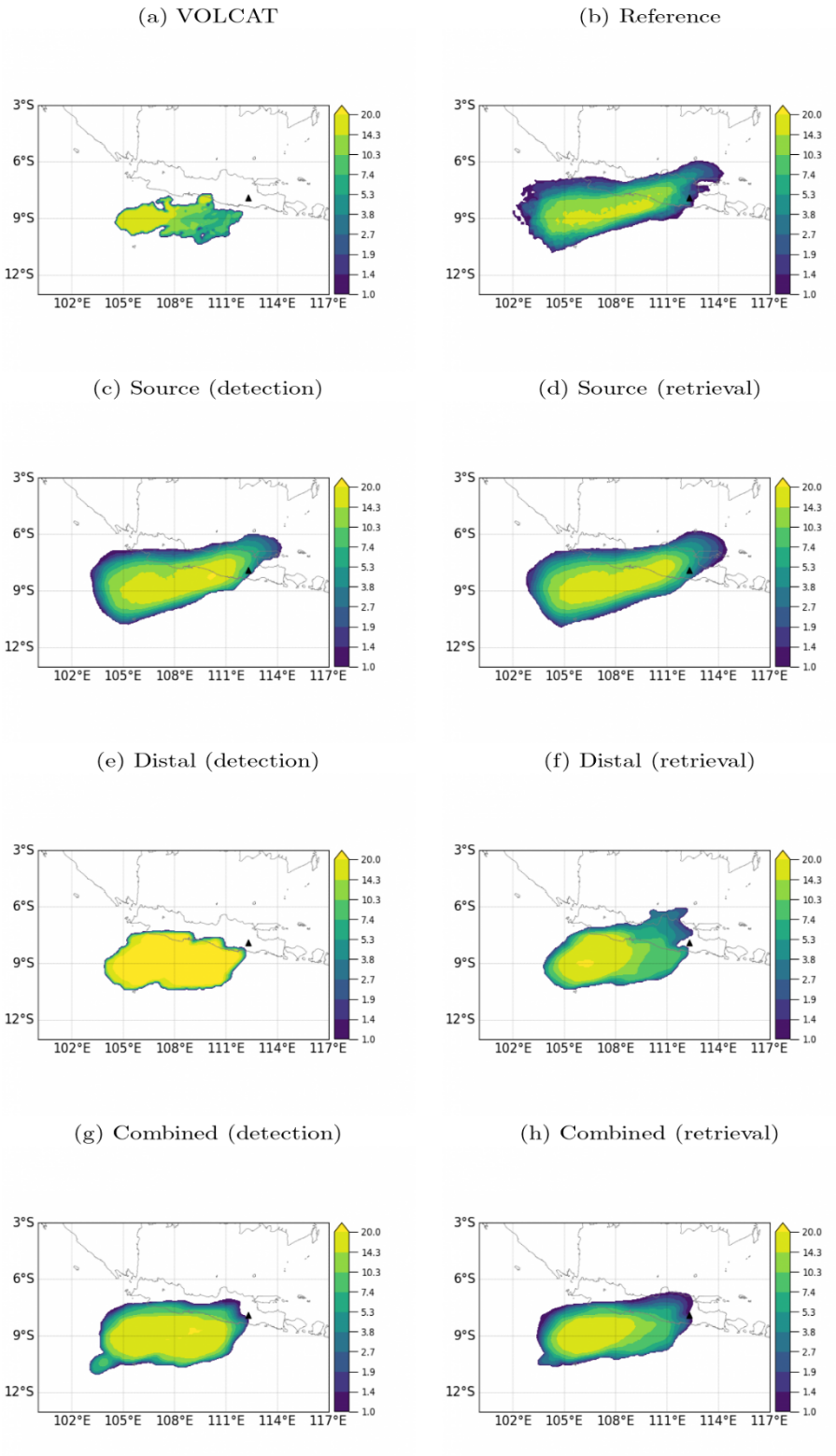

Figure S5. Ensemble mean cloud top height fields in the 13 February 2014 Kelut eruption case study at 14/0130 UTC for (**a**) VOLCAT retrieval, (**b**) reference run, (**c**) cylindrical source run with detection-based optimization, (**d**) cylindrical source run with retrieval-based optimizations, (**e**) distal source run with detection-based initialization and optimization, (**f**) distal source run with retrieval-based initialization and optimization, (**g**) hybrid source run using detections, and (**h**) hybrid source run using retrievals.

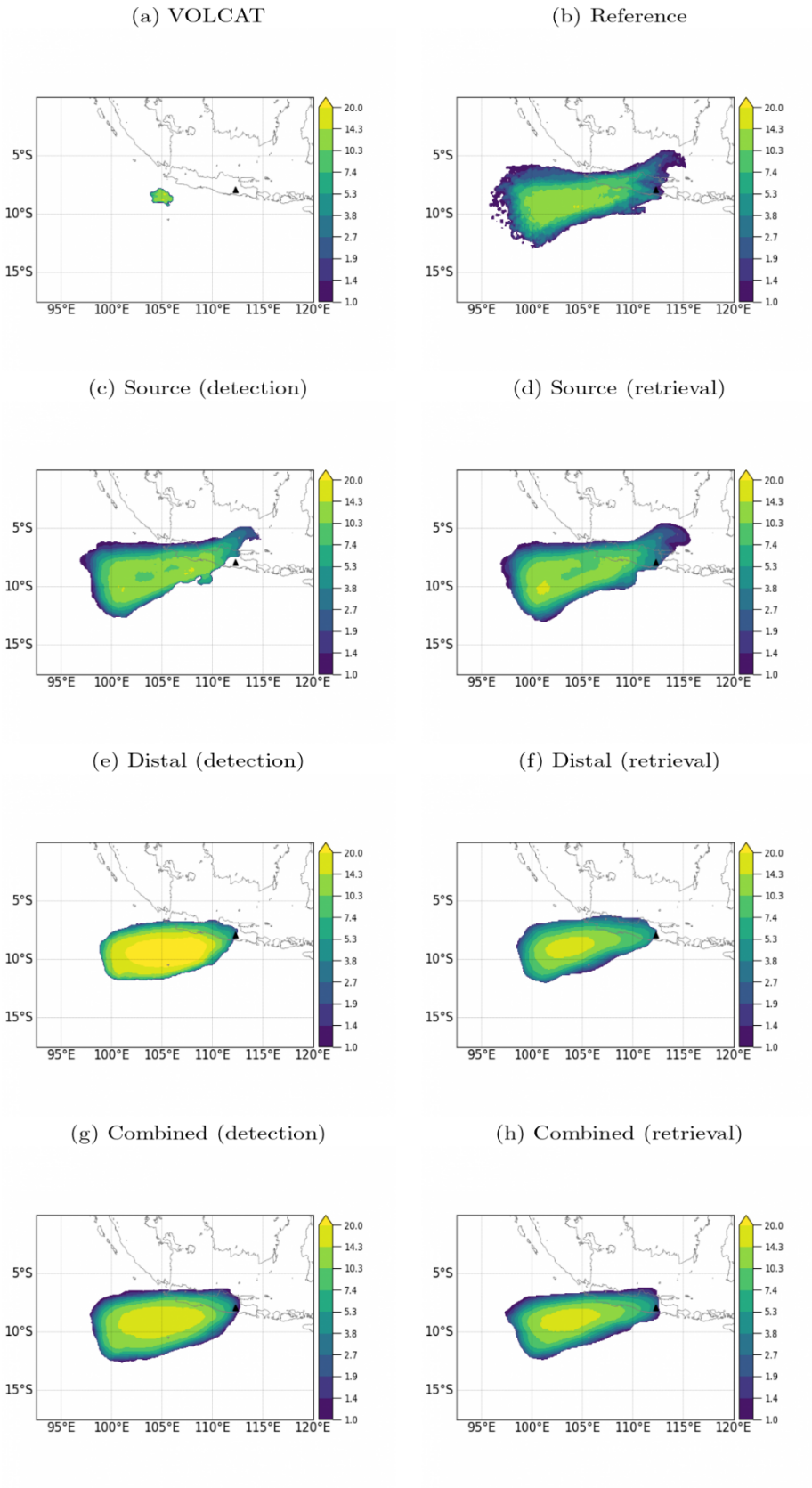

Figure S6. Same as in Figure S5 but for the 14/0830 UTC timestep.

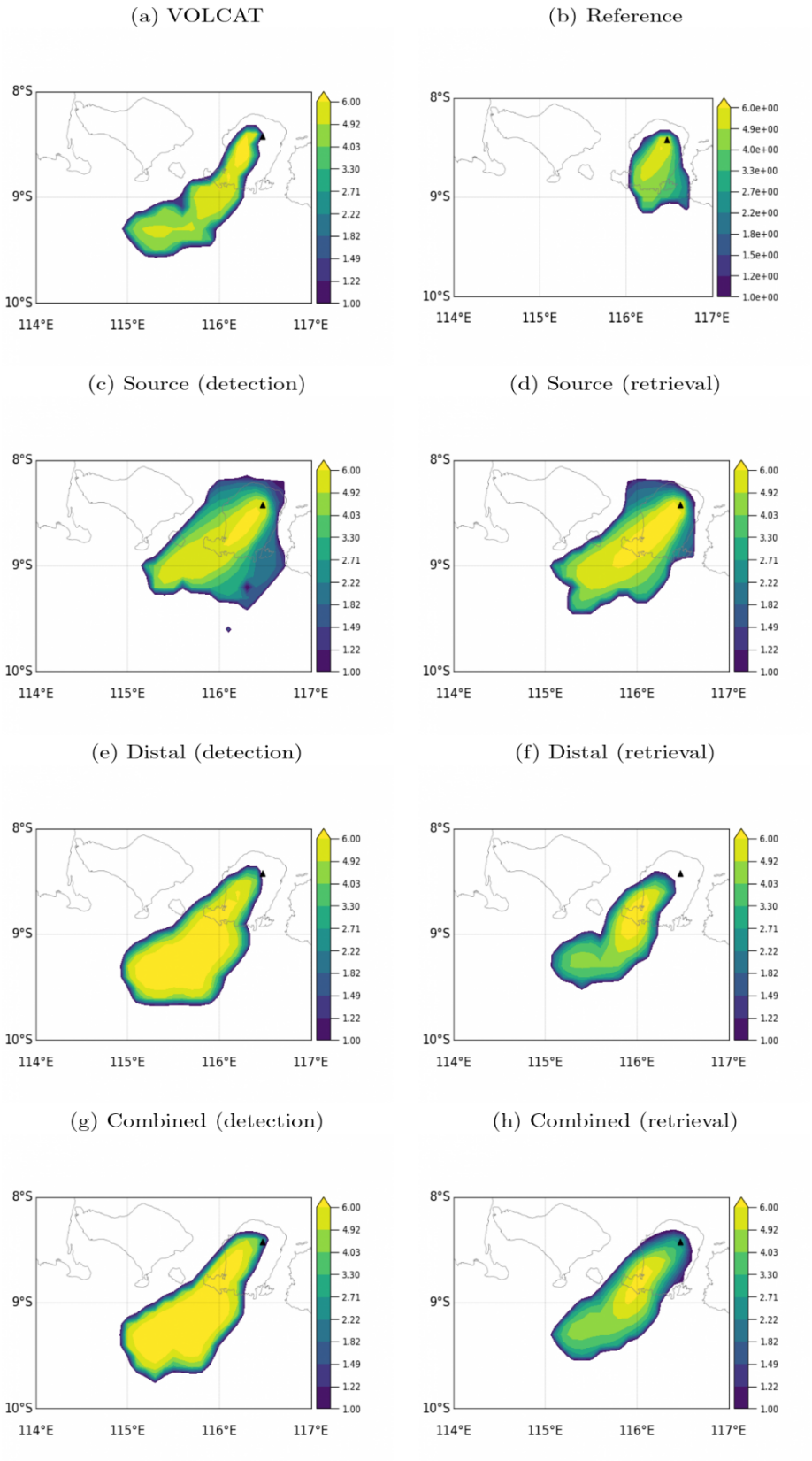

Figure S7. Same as in Figure S5 but for the 4 November 2015 Rinjani case study at 5/0730 UTC.

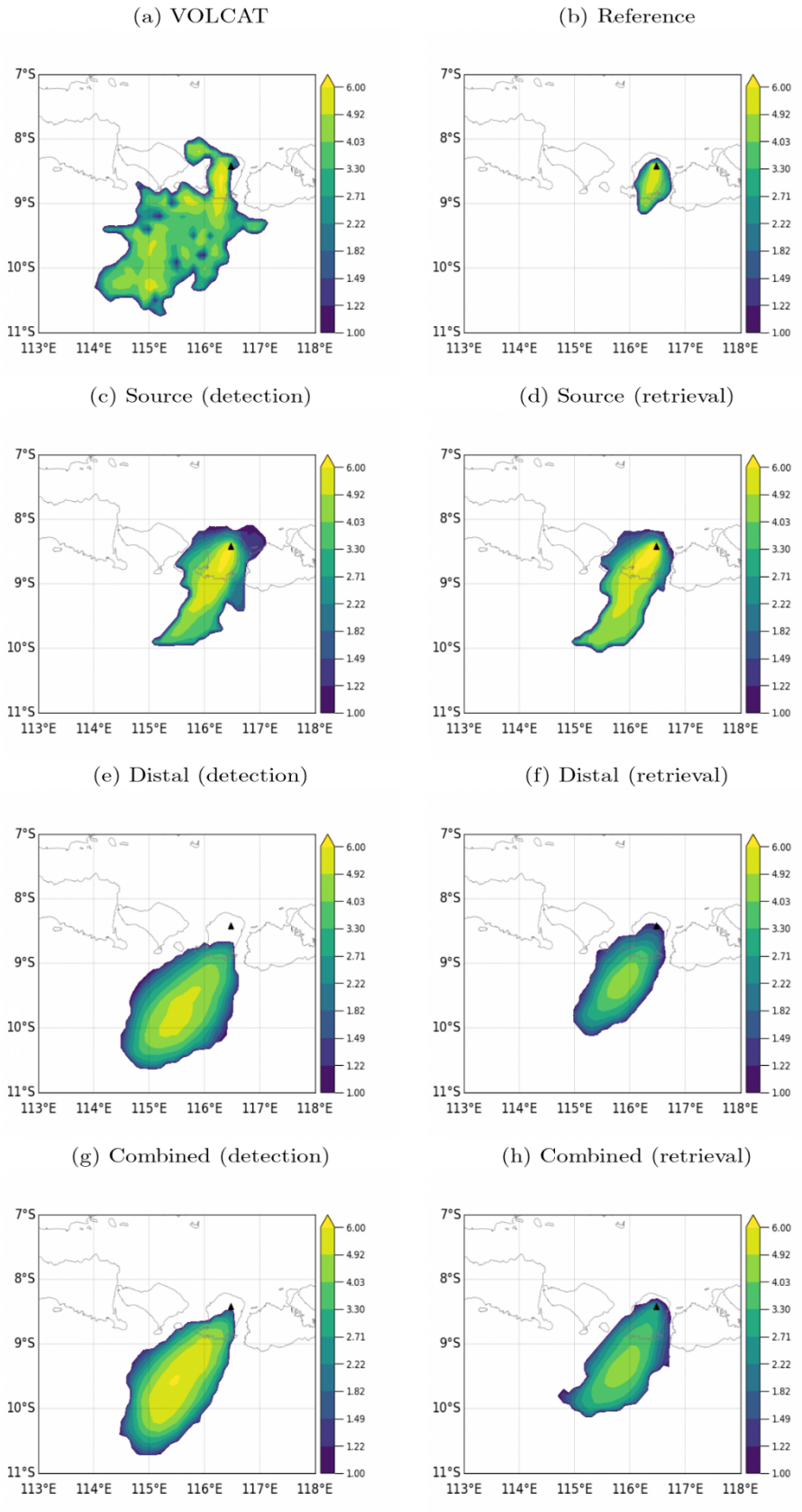

Figure S8. Same as in Figure S7 but for the 5/1430 UTC timestep.

3.2. 4 November 2015 Rinjani Eruption

Figure S7 shows the results from the Rinjani case study at 5/0730 UTC, which occurs during the analysis phase. The VOLCAT retrieval shows cloud top heights in the 5–6 km range over most of the ash cloud. The reference run reproduces these heights near the source, but the ash cloud does not extend far enough to the south-west. The cylindrical source runs (SRC) represent the cloud top heights quite well with reference to the retrievals. The distal source runs (DIST(VARH)) represent the ash cloud location better than either the reference of SRC runs, and the retrieval-based run also represents the variation of top height within the cloud quite well. The detection based DIST(VARH) run does not represent the variation very well (being uniform throughout the cloud), but the magnitude of the cloud top height is broadly consistent with that in the retrieval. The hybrid schemes (SRC-DIST) perform very similarly to the DIST schemes.

Figure S8 shows the results obtained in the Rinjani case study at 5/1430 UTC, which occurs during the forecast phase. The VOLCAT retrieval shows cloud top heights of around 6 km near the source as well as well small, isolated, regions downstream, most likely a manifestation of retrieval error. The reference run reproduces the cloud top heights quite well near the source, but it does not extend far enough downstream as noted previously. The ash cloud representation is somewhat better in the SRC runs and the cloud top heights agree reasonably well with the VOLCAT retrievals. The detection based DIST(VARH) run represents the extent of the ash cloud better, but the altitude near the source is underestimated; this is a consequence of the fact that in the distal formulation, emissions occurring after the initialization time are not represented. A similar deficiency can be noted in the retrieval-based run as well. The hybrid scheme runs (SRC-DIST) have similar representations of the ash cloud location, but they represent the ash released near the source better; this is especially noticeable in the detection-based run.

4. Conclusions

The simulated spatial pattern of effective radius is in general not very well correlated with the VOLCAT retrievals. The use of the distal source does improve the effective radius representation somewhat when compared to reference and cylindrical source runs during the analysis phase, but the improvement during the forecast phase is marginal. The simulated spatial patterns of cloud top heights have higher correlations with VOLCAT retrievals. However, the reference runs appear to already have decent skill with respect to the VOLCAT retrievals, so the improvement from ensemble filtering is only by a small margin. As for the effective radius field, improvements from using the distal source are more significant during the analysis phase, but they are less impressive during the forecast phase. In general, bigger improvements to both effective radius and cloud top height were noted for the Rinjani case study, suggesting that the distal formulation is better suited for lower-level and longer-lived eruptions. This is supported by the skill scores results in Figures S2 and S3 of the main manuscript.

References

1. Zidikheri, M.J.; Lucas, C. A computationally efficient ensemble filtering scheme for quantitative volcanic ash forecasts. *J. Geophys. Res. Atmos.* **2020**, e2020JD033094.
2. Pavolonis, M.J.; Heidinger, A.K.; Sieglaff, J.Automated retrievals of volcanic ash and dust cloud properties from upwelling infrared measurements. *J. Geophys. Res. Atmos.* **2013**, *118*, 1436–1458.
3. Hansen, J.; Travis, L. Light scattering in planetary atmospheres. *Space Sci. Rev.* **1974**, *16*, 527–610.
4. Zidikheri, M.J.; Lucas, C. Using satellite data to determine empirical relationships between volcanic ash source parameters. *Atmosphere* **2020**, *11*, 342.
5. Hobbs, P.V.; Radke, L.F.; Lyons, J.H.; Ferek, R.J.; Coffman, D.J.; Casadevall, T.J. Airborne measurements of particle and gas emissions from the 1990 volcanic eruptions of Mount Redoubt. *J. Geophys. Res.***1991**, *96*, 18735–18752.
6. Zidikheri, M.J.; Lucas, C.; Potts, R.J. Estimation of optimal dispersion model source parameters using satellite detections of volcanic ash. *J. Geophys. Res. Atmos.* **2017**, *122*, 8207–8232.